

## L'-BAND INTERFEROMETRIC OBSERVATIONS OF EVOLVED STARS

G. CHAGNON

Laboratoire d'Etudes Spatiales et d'Instrumentation en Astrophysique, Observatoire de Paris, 5, Place Jules Janssen,  
F-92195 Meudon, France; Gilles.Chagnon@obspm.fr

B. MENNESSON

Jet Propulsion Laboratory, MS 306-388, California Institute of Technology, 4800 Oak Grove Drive, Pasadena CA 91109

G. PERRIN, V. COUDÉ DU FORESTO, P. SALOMÉ, AND P. BORDÉ

Laboratoire d'Etudes Spatiales et d'Instrumentation en Astrophysique, Observatoire de Paris,  
5, Place Jules Janssen, F-92195 Meudon, France

AND

M. LACASSE AND W. TRAUB

Harvard-Smithsonian Center for Astrophysics, 60 Garden Street, Cambridge, MA 02138

Received 2002 March 14; accepted 2002 July 19

### ABSTRACT

Ten bright Miras, six semiregular variable giants, and two semiregular variable supergiants have been observed with the Infrared-Optical Telescope Array interferometer in the  $L'$  band (from 3.4 to 4.1  $\mu\text{m}$ ). Observations were carried out in 2000 March and November with the FLUOR/TISIS instrument, using optimized single-mode waveguides for optical recombination and a dedicated chopping system for accurate subtraction of slow thermal background drifts. Four of the sources (the Mira stars R Leo and R Cnc,  $\alpha$  Ori, and RS Cnc) were observed in both runs. We report on visibility measurements and derive  $L'$  broadband uniform disk (UD) diameter best fits for all 18 stars in our sample. We also detect strong departures from UD models in some peculiar cases.

*Key words:* stars: AGB and post-AGB — stars: late-type — techniques: interferometric

### 1. INTRODUCTION

The circumstellar environment of evolved stars shows complex structures, which are the results of the peculiar story and physical conditions of each individual star. These can appear as hot spots (Young et al. 2000), departures from symmetry (as shown in *HST* images of  $\alpha$  Ori in Gilliland & Dupree 1996), and as strong temporal (Perrin et al. 1999; Burns et al. 1998; Thompson, Creech-Eakman, & van Belle 2002) and chromatic size variations (Tuthill, Haniff, & Baldwin 1999a; Tuthill, Monnier, & Danchi 1999b, 2000).

It is then necessary to gather data from star samples as large as possible—to look for possible general trends and exceptions—with maximum temporal and spectral coverage. In this context, high angular resolution observations of circumstellar dust shells in the thermal infrared are particularly interesting, because contributions from the upper colder atmospheric layers (molecules and/or dust) become detectable against the classical photospheric emission.

Interferometric measurements have already been achieved in the thermal infrared with the ISI heterodyne interferometer (Danchi et al. 1994; Hale et al. 2000) at 11.15  $\mu\text{m}$ . At this wavelength, with the resolution provided by its maximum baseline (now 75 m) and its narrow bandwidth imposed by the heterodyne technique, ISI mainly focuses on dust shell properties of bright late-type stars.

In order to carry out wide-band two-telescope observations in the thermal infrared, the TISIS experiment (working at 3.8  $\mu\text{m}$ ) was designed as an extension of the FLUOR instrument (working at 2.2  $\mu\text{m}$ ) on the Infrared-Optical Telescope Array (IOTA) interferometer. It made possible the first  $\sim 20$  mas angular resolution stellar observations in this wavelength domain (Mennesson et al. 1999).

It was also a first step toward direct interferometry at even longer thermal infrared wavelengths, as required for space-based observatories with the DARWIN project (Léger et al. 1996) or ground-based arrays of telescopes, such as the Very Large Telescope Interferometer with its mid-infrared instrument MIDI (Leinert & Graser 1998) or the Keck telescopes with the 10  $\mu\text{m}$  nulling mode (Colavita et al. 1998).

The aim of previous articles (Mennesson et al. 1999, 2000) was to introduce the very first results obtained with the instrument. The current work will present its most recent results, since the instrument has become fully functional on IOTA. We mainly aim here at summarizing our  $L'$  visibility measurements for future reference and analysis. Detailed interpretation and modeling of the data is beyond the scope of this work. This will be addressed in forthcoming papers, as illustrated by our analysis of observed chromatic stellar size variations between  $K'$  and  $L'$  bands (Mennesson et al. 2002).

After a brief description of the experimental setup, we will present the observations and the reduction process. The results will then be detailed before a few comments on individual stars of particular interest among the observations.

### 2. FLUOR/TISIS

#### 2.1. General Presentation

The observations were carried out with two 45 cm telescopes of the IOTA interferometer located on Mount Hopkins, in Arizona. A complete description of IOTA is given in Traub (1998). In each of the telescopes, the direction of the beam is corrected for the rapid tip-tilt motion introduced by the atmosphere. This servo-looped stabiliza-

tion is based on the stellar image centroid position measured by visible star trackers. The external path differences between the beams are compensated by two delay lines introducing a variable delay in one arm. The interferometer delivers in its central laboratory a pair of stabilized and properly delayed afocal beams, which in our case were combined on the TISIS table. The telescopes can be relocated over an L-shaped set of stations providing baselines ranging in length from 5 to 38 m.

## 2.2. Specific Setup for the Thermal Infrared

Details on the setup itself have already been given in Mennesson et al. (1999). We only describe in the present paper the upgrades that we implemented with respect to the initial 1999 observational setup.

### 2.2.1. Modifications to the FLUOR Optics

A major improvement of TISIS since the first observations has been the use of a  $L'$ -band-dedicated single-mode coupler, replacing the previous coupler, which was optimized for the  $K$  band. Since it is an X-coupler, the guided optics equivalent of a beam splitter, it does not provide any photometric output. The bandpass of the filter (which is the same one as in the first observations with TISIS) extends from 3.4 to 4.1  $\mu\text{m}$ , with an effective wavelength  $\lambda_{\text{eff}} = 3.77 \mu\text{m}$ .

### 2.2.2. Detector

TISIS uses InSb photometers whose sensitivity extends to the  $M$  band, beyond the limits of the NICMOS camera with which FLUOR is now operated. Their noise equivalent power is of the order of  $10^{-14} \text{ W Hz}^{-1/2}$ . One photometer was available in 2000 March, and two for the 2000 November run. This makes the visibility measurements of this latter run more robust, since they are based on two interferometric outputs.

### 2.2.3. Chopping System

One of the main characteristics of observing in the  $L'$ -band, compared with the  $K$ -band, is the larger thermal background due to the blackbody emission of the optical train of the interferometer and to the emission of mostly water vapor in the atmosphere. It is necessary to subtract this contribution from the mean value of the interferogram in order to not bias the continuum estimate. This background depends on time first because the water vapor content on the line of sight and the temperature of the optical train change during the night and second because, as one switches from one star to another one (for example, from a reference star to an astronomical source), optical beams may hit different parts of the optics with different temperatures and emissivities.

The usual means to subtract the instrumental contribution to the background is known as chopping. “Standard” chopping systems tilt the secondary mirror of the telescope of a few arcseconds at a frequency of a few hertz. As this procedure cannot be operated on IOTA, we had to implement a simple system to force the siderostats to offset from the star from time to time.

We use the fact that on IOTA, star tracking is achieved by separating the visible part of the beams and sending it on dedicated CCD cameras. As said above, a servo loop controls tip-tilt mirrors to ensure that the stellar centroid

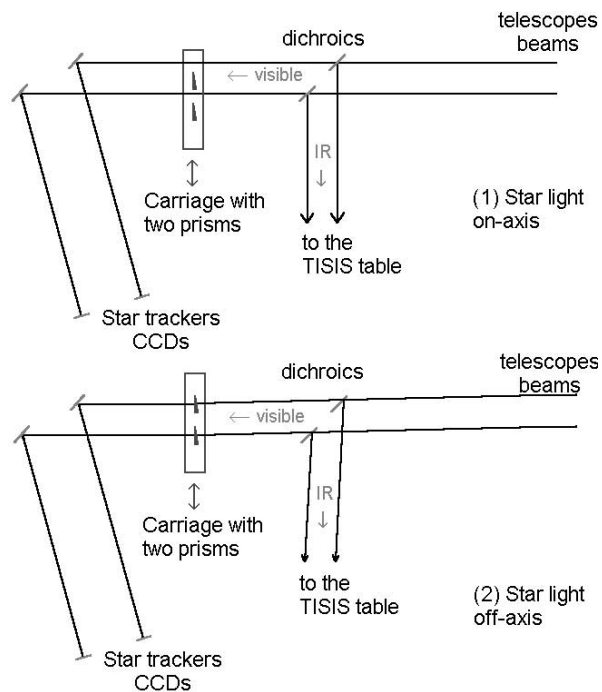


FIG. 1.—Schema of the chopping system installed on IOTA. Details are given in the text (see § 2.2.3).

position stays at a fiducial point in the CCD plane. We have inserted in the visible beams a carriage that supports two wedged glass plates (one per beam) that provide a deviation by an angle of a few arcseconds of the beams. This carriage can move in (Fig. 1, case 2) and out (Fig. 1, case 1) of the beams. When the prisms intercept the beams, the star-trackers are misled over the actual position of the star and thus offset the telescopes in a fixed direction. The offset provided on the sky by this system is about  $9''$  for the data acquired in 2000 March and  $18''$  for the 2000 November data (see the sections dedicated to the description of the observations for further details about the modification of the offset we were lead to apply).

### 2.2.4. Limiting Magnitude

The current limiting magnitude ( $L \approx -1$ ) is set by the detector’s noise only. Further improvements in limiting magnitude will be possible with better detectors, up to the point where thermal background fluctuations will start dominating the detector noise. The theoretical background limited magnitude is expected to be close to zero (Mennesson et al. 1999). Most of the accessible bright stars ( $L < -1$ ) have already been observed. In order to access fainter stars, faster chopping schemes would also be necessary to provide reliable visibility measurements.

## 3. OBSERVATIONS AND REDUCTION

### 3.1. Observations

#### 3.1.1. 2000 March

##### 3.1.1.1. Chopping System

A first version of the chopping system was implemented in 2000 March. In theory, a relative deviation of a few times the size of the Airy disk seen by the fiber should have been

sufficient. In the  $L'$  band, with the IOTA telescopes, this represents a few times  $1''$ . We therefore used prisms that applied a  $9''$  deviation to the beams.

### 3.1.1.2. System Limitations

The deviation of  $9''$  appeared not to be sufficient, since the reduction of the data showed that a contamination by the stellar flux could be noticed in the off-source signals, especially for the brightest stars. This could have been critical, since these data were planned to be used as an estimate of the thermal background. The relative amount of the contamination varied a lot from night to night and even between the beginning and the end of the same night. We suspected this phenomenon to be caused by the seeing, and the fact that the tip-tilt correction system of IOTA was not able to perfectly correct the wavefront, which entailed slight movements of the star image at the fiber input.

### 3.1.1.3. Solutions

A fringe contrast is fundamentally a modulation amplitude divided by a continuum. If there is an error in the estimate of the continuum, as that is the case when the determination of the background level is biased by stellar contamination, then it directly propagates into the estimate of the contrast. Fortunately, a stellar contamination is proportional to the stellar flux, which is the continuum used as a reference in the contrast estimate. This implies that if the error is the same for the source and the calibrator, its effect disappears. This requires that the mean seeing does not vary between the source and the calibrator. No such variation is noticed in the data. Moreover, should such a variation have occurred, estimates on the calibrator before and after the source would not have been consistent. Since such a variation is interpreted in the reduction process as a variation of the interferometer transfer function, the effect of a seeing variation in the determination of the background level is taken into account, at least to the first order.

However, this is one reason why the 2000 March data are expected to be of poorer quality than those of the next run of observations in 2000 November.

## 3.1.2. 2000 November

### 3.1.2.1. Chopping System Improvement

The photometric contamination became apparent to us after the analysis of the 2000 March data. For the following run of observations, we removed this bias by increasing the amount of deviation that was applied to the visible beams. The deviation was increased up to  $18''$  by inserting one more

TABLE 1  
LIST OF THE 2000 MARCH CALIBRATORS

Reference Star	Spectral Type	$L'$ Mag	UD (mas)
$\alpha$ Boo <sup>a</sup> .....	K1.5 III	-3.1	20.39 $\pm$ 0.10
$\gamma$ Dra <sup>a</sup> .....	K5 III	-1.5	9.91 $\pm$ 0.25
$\mu$ Gem <sup>a</sup> .....	M3 III	-2.0	13.63 $\pm$ 0.15
$\delta$ Vir <sup>b</sup> .....	M3 III	-1.4	10.15 $\pm$ 0.55

<sup>a</sup> From di Benedetto & Rabbia 1987.

<sup>b</sup> Photometric measurements.

TABLE 2  
LIST OF THE 2000 NOVEMBER CALIBRATORS

Reference Star	Spectral Type	$L'$ Mag	UD (mas)
$\beta$ And <sup>a</sup> .....	M0 III	-2.1	14.40 $\pm$ 0.13
$\alpha$ Cet <sup>b</sup> .....	M1.5 IIIa	-1.9	12.08 $\pm$ 0.60
$\beta$ Gem <sup>a</sup> .....	K0 IIIb	-1.2	7.76 $\pm$ 0.30
$\mu$ Gem <sup>a</sup> .....	M3 III	-2.0	13.63 $\pm$ 0.15
$\alpha$ Hya <sup>a</sup> .....	K3 II-III	-1.4	9.11 $\pm$ 0.46
$\beta$ Peg <sup>a</sup> .....	M2.5 II-III	-2.4	16.33 $\pm$ 0.23
$\alpha$ Tau <sup>a</sup> .....	K5 III	-3.0	20.24 $\pm$ 0.22

<sup>a</sup> From di Benedetto & Rabbia 1987.

<sup>b</sup> Photometric measurements.

deviating plate in each beam. No photometric contamination of the background was detected in the data acquired during this run.

### 3.1.3. Calibrators

For our set of calibrators, we started with  $K'$ -band uniform disk (UD) diameters derived from previous interferometric measurements (di Benedetto & Rabbia 1987; Perrin et al. 1998) or from photometric measurements, which yield a typical uncertainty of 5% (Perrin et al. 1998). We then derived the expected  $L'$  apparent UD diameters by computing the theoretical differential limb darkening between the  $K'$  and  $L'$  bands. For each band and each calibrator spectral type, we used the corresponding limb-darkening coefficients computed by Manduca (1979). Tables 1 and 2 present the calibrators that were used respectively in the March and November missions.

## 3.2. Reduction

The data are reduced basically following the standard FLUOR procedure, described in Coudé du Foresto, Ridgway, & Mariotti (1997) and Perrin et al. (1998). However, a few modifications had to be made to take into account the fact that no photometric channel was available and the necessity of dealing with the background level.

### 3.2.1. Photometric Fluctuations Correction

Phase fluctuations of the wavefront at the entrance of a monomode fiber are translated into temporal fluctuations of the flux at the output and contaminate the interferogram. In the FLUOR instrument, the monitoring is performed with the help of two photometric channels provided by a triple-fibered coupler (Coudé du Foresto et al. 1998). Only one X-coupler is available for the TISIS setup, so this technique cannot be used. The estimate of these fluctuations is alternatively performed with the lowest frequencies part of the interferometric channels. This approximation yields additional bias on the contrast estimate, as described in Coudé du Foresto et al. (1997), but this bias disappears in the calibrated visibility, provided the photometric unbalance between the two beams does not vary when one switches from the calibrator to the scientific target. This point was addressed as carefully as possible during the observations by monitoring the balance between the mean photometric levels in each beam. Proper balance is ensured by an optimized injection in the fibers. In addition, the bias introduced by different brightness ratios seen on the calibra-

tor and on the source is very small. If the two beams to be interfered are seen with a 1.5 brightness ratio on the source and then at 1.0 on the calibrator, the visibility is biased by 2%. We never saw such radical brightness ratio changes during the observations.

### 3.2.2. Background Subtraction

#### 3.2.2.1. Observing Procedure

A standard acquisition sequence for TISIS consists for both runs of one on-source “batch” bracketed by two off-source batches acquired on the sky 9” or 18” away from the star.

1. Each on-source batch consists of about 100–200 interferograms for the data acquired in 2000 March and 60 for the data acquired in 2000 November, allowing faster background measurements.

2. Each off-source batch consists of about 100 scans for the 2000 March data and 60 scans for the 2000 November data.

#### 3.2.2.2. Removal of the Drift in the Thermal Background

As the chopping frequency is quite low (about 0.01 Hz), it is necessary to take into account a possible variation of the background; this is done by performing the following operations:

1. A mean value is computed for each off-source scan;
2. the sequence of measurements made of the two off-source batches is linearly fitted; and
3. the result of the fit is subtracted from each interferogram.

Figure 2 illustrates this procedure. Although the real variation of the background is obviously not linear in time, the performed approximation allows us to remove its most important contribution to the continuum. This is similar to the way the fluctuations of the transfer function of the instrument is estimated between each observation of a calibrator. The performed approximation is validated by the fact that in most cases, the rms of the fluctuations observed during the “off-source” batches stays within a few percent of the stellar signal for the faintest sources. Figure 2 gives an example: the stellar signal is about 2300 units, and the rms

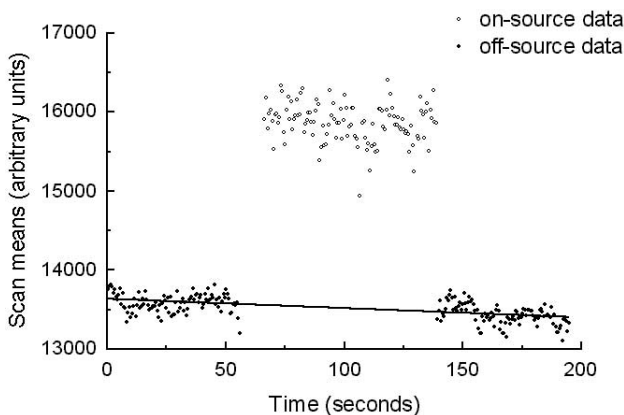


FIG. 2.—Thermal background subtraction. The means of the off-source batches are linearly fitted; the result of the fit is then subtracted from the on-source data ( $\alpha$  Boo, 2000 March 14).

of the off-source data after subtraction of the fit is about eight for the bright star  $\alpha$  Boo. This is compatible with the discrepancies that appear between the data points and the best-fitting curves.

### 3.3. Data Selection Criteria

#### 3.3.1. Background Subtraction

In some cases, the linear approximation is clearly not valid, mainly because the background variation is inconsistent between the two off-source batches (for instance, the signs of the slopes differ). This results in a noticeable remaining increase or decrease in the contrast estimates for the individual interferograms over the whole on-source batch. The corresponding data are rejected.

#### 3.3.2. Transfer Function Estimate

Some of the 2000 March data show an apparent instability of the interferometer transfer function. A criterion has been defined, based on the amount of the variation and the time interval between the calibration observations. The uncertainty on the reference star diameter leads to an uncertainty in the instantaneous value of the transfer function. Let  $T_0$  and  $T_1$  be the values of the transfer function computed with the contrast measured on the reference star, respectively, before and after the observation of the source, and let  $\epsilon_0$  and  $\epsilon_1$  be their respective uncertainties. The time interval between the bracketing calibration observations is  $\tau$ . One then defines one parameter  $\alpha$  as

$$\alpha = (T_1 - T_0) / \tau \epsilon_0.$$

The data are rejected if  $\alpha > 0.5 \text{ min}^{-1}$ . This value is not based on a priori statistical considerations on the stability of the transfer function but is empirically determined. Its exact value is not critical, since the fluctuations of the transfer function induced by this observing procedure are quite strong and the phenomenon unambiguous.

## 4. RESULTS AND DISCUSSION

### 4.1. General Considerations for Each Run

#### 4.1.1. 2000 March

Thirty-seven visibility points out of a total of 59, acquired in five nights, have finally been kept for this run. The visibility curves are given in Figures 3 and 4.

Error bars on the visibilities that are given in Table 3 are formal errors given by the standard FLUOR-like reduction procedures, as they are described in Coudé du Foresto et al. (1997). The fact that only one interferometric output was available in the 2000 March data has been taken into account.

#### 4.1.2. 2000 November

Sixty-eight visibility points out of a total of 89, acquired in eight nights, have finally been kept for this run. The visibility curves are given in Figures 5 and 6.

Tables 4 and 5 show the data points for the 2000 November mission. Both interferometric channels were available for most of these observations.

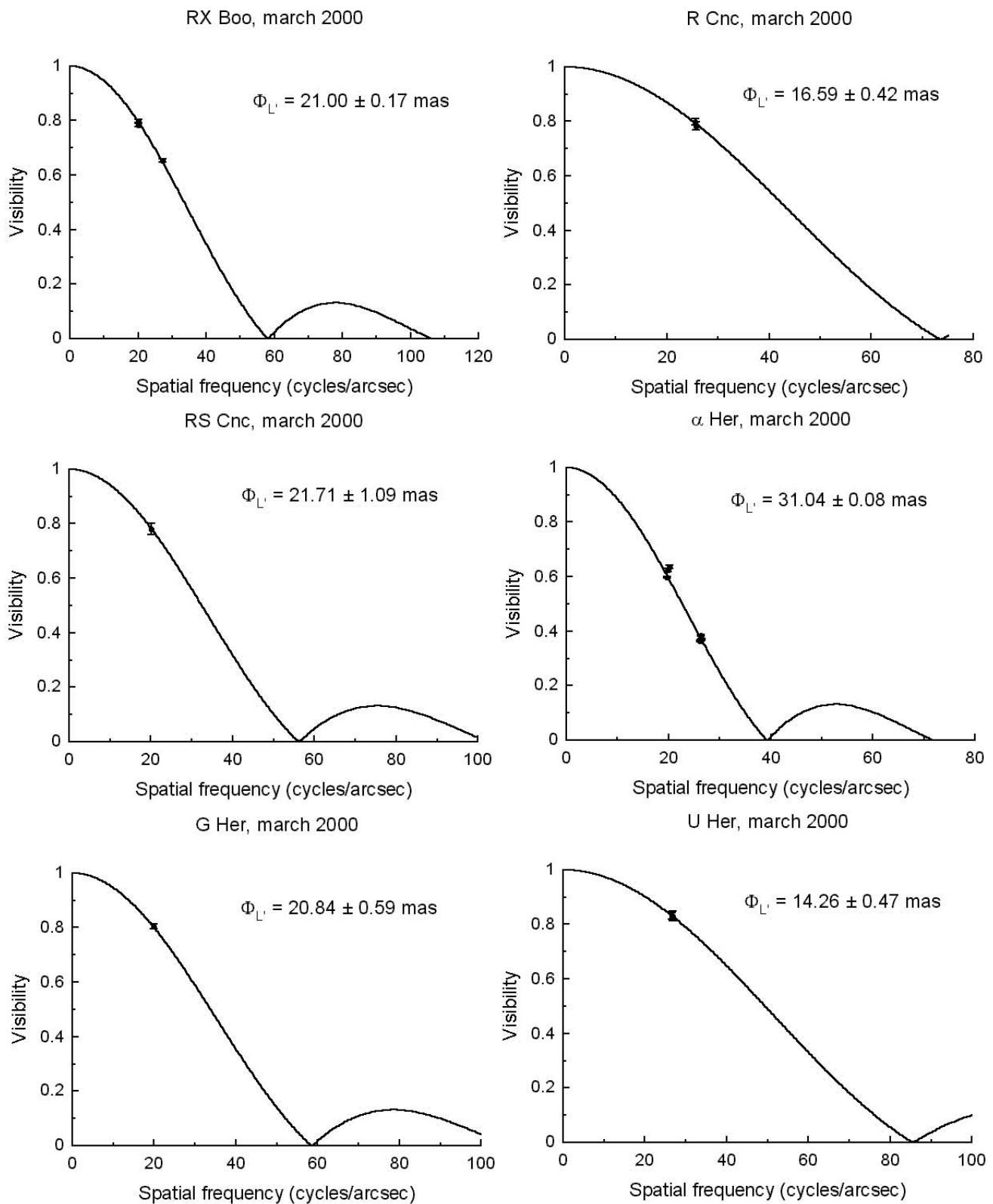


FIG. 3.—Visibility curves and best-fitting UD diameters for the 2000 March sources (from RX Boo to U Her)

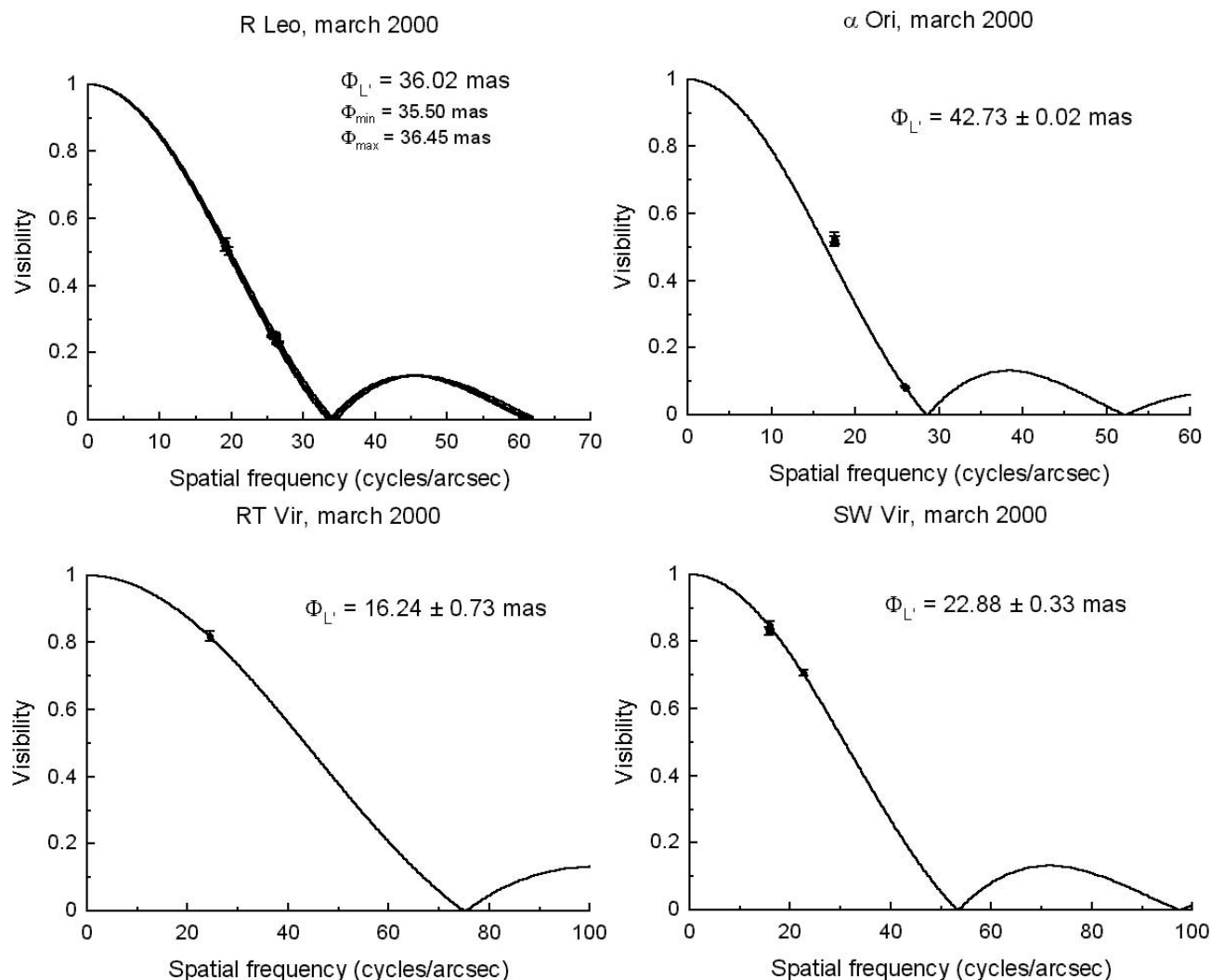


FIG. 4.—Same as Fig. 3, but from R Leo to SW Vir

## 4.2. UD Model Diameters

### 4.2.1. Rationale

We have chosen to present UD model diameters in this paper. We are aware that deviations from such a simplified model are expected from the stars of the sample. However, it allows us to provide a simple, single parameter to serve as an estimate of the “typical size” of the star.

### 4.2.2. Fitting Accuracy

The accuracy of the fitting mainly depends on two factors:

1. underestimations of some of the error bars on the visibilities (this is more likely to be expected for the March data); and
2. the simplicity of the model itself for some of the stars in our sample.

Moreover, for a few stars (R Aqr, RS Cnc in March, g Her, and RT Vir), only one data point is available. For some others (R Cnc, U Her, R Lep, R LMi, and  $\rho$  Per), data were acquired at only one spatial frequency. More complex structures than those of a single-parameter model such as a UD model cannot, therefore, be noticeable.

Those remarks lead us to consider different ways of presenting the results of the fits, according to the nature of the available data.

### 4.2.3. Results

The reduction procedure provides for a set of data one UD diameter, the reduced  $\chi^2$  of the fit, and an error bar, which is computed by varying the  $\chi^2$  of the fit until it increases to  $\chi^2_{\min} + 1$  (Perrin et al. 1998).

Three categories of stars can then be considered:

1. The stars for which only one data point is available, or for which the  $\chi^2$  of the fit is smaller than one. The diameter given in Table 6 is the one given by the reduction procedure.
2. The stars for which  $\chi^2 > 1$  and no important departure from a UD model is noticeable or expected. This is, in particular, the case for the supergiants  $\alpha$  Her and  $\alpha$  Ori. The error bars on the diameter given in Table 6 are increased in order to force the  $\chi^2$  of the fit to one.
3. The stars for which  $\chi^2 > 1$  and that clearly depart from a UD model. In this case, Table 7 gives three diameters: the smallest UD diameter fitting at least one data point, the best fitting UD, and the greatest UD fitting at least one data point.

TABLE 3  
 2000 MARCH DATA POINTS

Star	Spectral Type	UT Date	Julian Date	Phase	Spatial Frequency (cycles arcsec <sup>-1</sup> )	Azimuth <sup>a</sup> (deg)	Visibility (%)
RX Boo.....	SR M7.5	Mar 10	51,614	0.50	27.24	104.58	65.3 ± 0.6
		Mar 12	51,615	0.51	20.13	71.40	78.4 ± 0.5
		Mar 12	51,616	0.51	20.08	73.38	79.9 ± 0.5
R Cnc.....	Mira M7 IIIe	Mar 11	51,614	0.37	25.61	91.08	79.9 ± 1.1
		Mar 11	51,614	0.37	25.66	94.60	78.3 ± 1.4
		Mar 14	51,617	0.77	20.20	99.05	78.1 ± 2.0
RS Cnc.....	S M6 IIIa se	Mar 14	51,617	0.77	20.20	99.05	78.1 ± 2.0
α Her .....	SR M5 Ib–II	Mar 9	51,613	...	26.45	75.64	36.9 ± 0.4
		Mar 9	51,613	...	26.38	76.90	36.6 ± 0.4
		Mar 9	51,613	...	26.29	78.68	38.4 ± 0.4
		Mar 9	51,613	...	26.22	80.14	36.3 ± 0.4
		Mar 12	51,616	...	19.78	63.40	59.7 ± 0.3
		Mar 14	51,618	...	20.19	57.81	63.6 ± 0.6
		Mar 14	51,618	...	19.88	62.10	62.5 ± 0.5
		Mar 12	51,616	0.55	19.83	61.47	80.3 ± 1.0
g Her.....	SR M6 III	Mar 12	51,616	0.55	19.83	61.47	80.3 ± 1.0
U Her.....	Mira M8 IIIe	Mar 10	51,613	0.27	26.76	79.32	83.1 ± 1.9
		Mar 10	51,614	0.27	26.69	96.64	83.1 ± 1.2
R Leo.....	Mira M8 IIIe	Mar 10	51,614	0.81	25.65	96.07	25.3 ± 0.3
		Mar 10	51,614	0.81	26.03	103.86	25.8 ± 0.3
		Mar 10	51,614	0.81	26.12	105.20	24.5 ± 0.2
		Mar 10	51,614	0.81	26.15	105.55	25.1 ± 0.3
		Mar 10	51,614	0.81	26.20	106.15	24.6 ± 0.2
		Mar 10	51,614	0.81	26.23	106.58	24.8 ± 0.2
		Mar 11	51,615	0.81	25.58	86.66	24.9 ± 0.2
		Mar 11	51,615	0.81	26.24	106.74	22.7 ± 0.2
		Mar 11	51,615	0.81	26.59	110.85	22.9 ± 0.3
		Mar 14	51,618	0.82	19.56	62.78	50.4 ± 1.3
		Mar 14	51,618	0.82	19.13	67.44	52.8 ± 1.1
		Mar 14	51,618	0.82	19.05	68.48	51.5 ± 1.1
		Mar 11	51,614	...	25.85	108.69	8.5 ± 0.1
		Mar 11	51,614	...	26.04	110.40	8.1 ± 0.1
Mar 14	51,617	...	17.62	81.08	52.1 ± 1.1		
Mar 14	51,617	...	17.45	88.85	51.7 ± 1.5		
Mar 14	51,617	...	17.45	89.49	52.8 ± 1.4		
RT Vir .....	SR M8 III	Mar 11	51,614	0.14	24.44	95.07	81.8 ± 1.5
SW Vir .....	SR M7 III	Mar 9	51,612	0.34	22.69	98.57	70.6 ± 0.8
		Mar 14	51,617	0.37	15.87	75.39	84.8 ± 1.2
		Mar 14	51,617	0.37	15.82	76.01	83.0 ± 1.2

<sup>a</sup> The azimuth is defined as the position angle of the projected baseline on the sky.

#### 4.3. Influence of Spectral Features

Warm molecular envelopes have been evidenced by *Infrared Space Observatory* infrared spectra of one Mira star (*o* Cet) and several M giants (e.g., SW Vir and RT Vir) of our sample (Yamamura, de Jong & Cami 1999; Tsuji et al. 1997). Spectral features due to molecular species in the envelope may bias the apparent angular size of the central star, either by an additional brightness of a region of the envelope, or by modifying the “effective wavelength” of the observations and thus the theoretical spatial frequency. However, it is not the purpose of this paper to study in details the influence of such features on the computed UD diameters. Moreover, preliminary studies by some of us tend to show that the continuum emission would play a more critical role in the interpretation of the observations. As said above, this will be addressed in forthcoming papers, as illustrated by our analysis of observed chromatic stellar size variations between  $K'$  and  $L'$  bands (Mennesson et al. 2002).

## 5. INDIVIDUAL COMMENTS

### 5.1. Miras Stars

One general result should be emphasized: all but one (U Ori) of the Mira stars in our sample for which data are available at high spatial frequencies show a departure from the UD model.

#### 5.1.1. *R Leo*

The quality of the data for R Leo is very good and stable. The variation between March and November is obvious, as shown in Figure 7. The same effect had already been observed with FLUOR in the  $K$  band, in 1997 and 1998 (Perrin et al. 1999), between phases 0.24 and 0.28.

The November data show excess at medium and high spatial frequencies, which is not the case in March. Moreover, the highest spatial frequency part of the November curve seems to connect with the UD model curve of the March data: the same relative amount of energy, in other words, would be present at the highest spatial frequencies in March

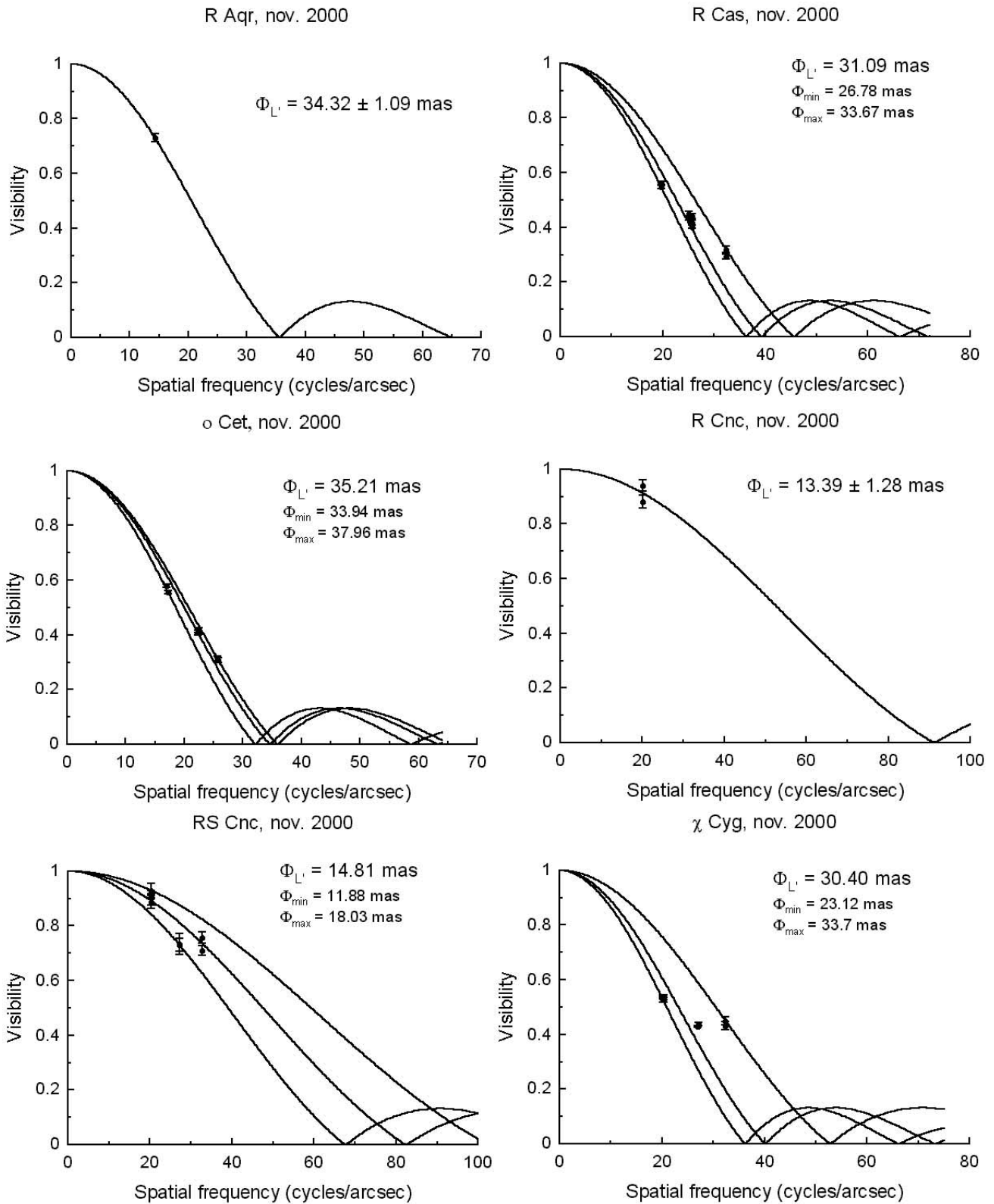


FIG. 5.—Visibility curves and best-fitting UD diameters for the 2000 November sources (from R Aqr to  $\chi$  Cyg)

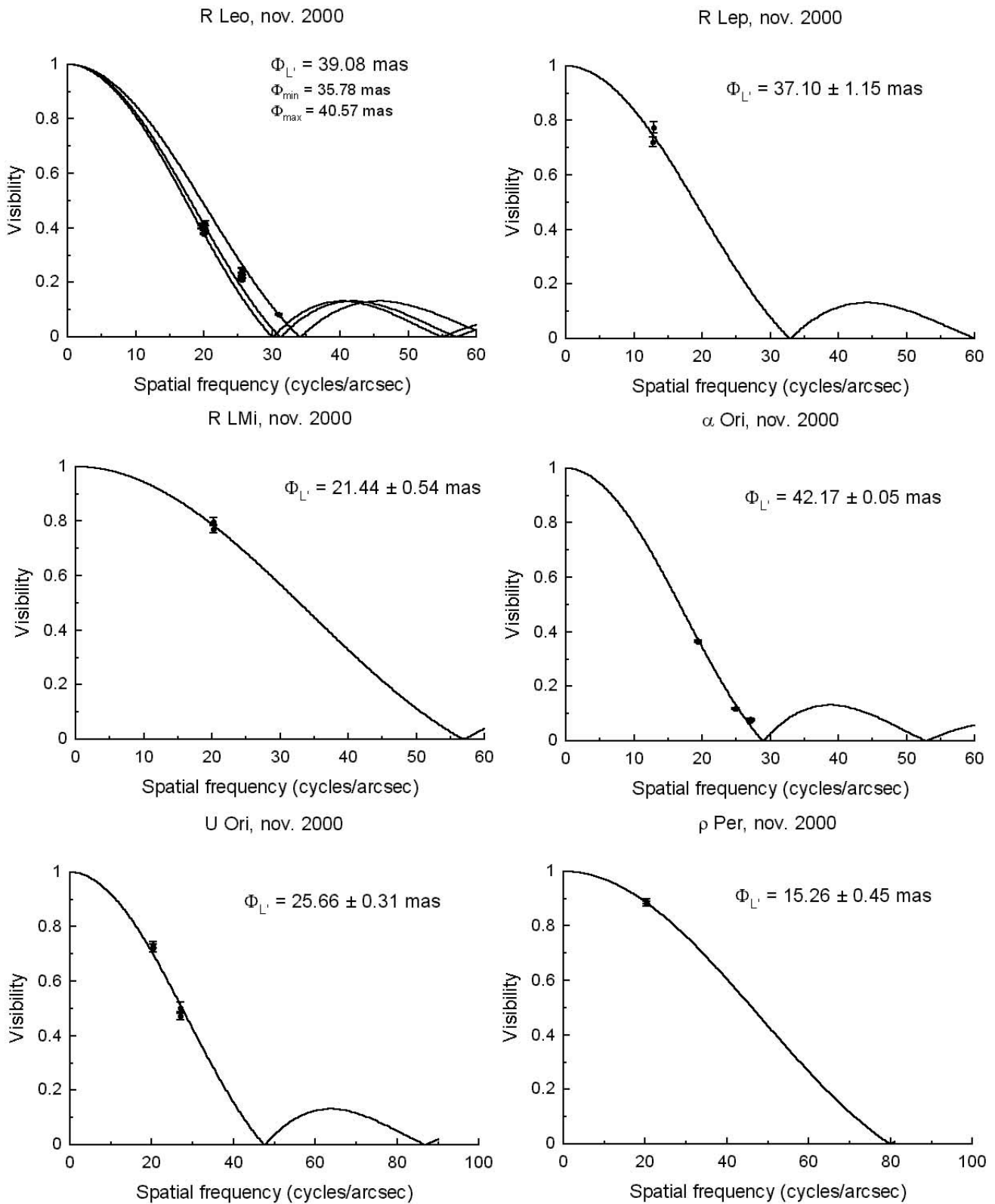


FIG. 6.—Same as Fig. 5, but from R Leo to  $\rho$  Per

TABLE 4  
2000 NOVEMBER DATA POINTS (FROM R AQR TO  $\chi$  CYG)

Star	Spectral Type	UT Date	Julian Date	Phase	Spatial Frequency (cycles arcsec <sup>-1</sup> )	Azimuth (deg)	Visibility (%)		
R Aqr.....	Mira M7 III pe var	Nov 20	51,868	0.41	14.30	61.74	73.1 ± 1.5		
R Cas.....	Mira M7 IIIe	Nov 14	51,862	0.16	25.71	92.45	40.1 ± 0.5		
		Nov 17	51,865	0.17	25.10	109.98	45.1 ± 0.8		
		Nov 17	51,865	0.17	25.08	109.27	43.2 ± 0.7		
		Nov 18	51,866	0.17	25.65	96.56	44.0 ± 0.8		
		Nov 18	51,866	0.17	25.65	96.84	41.5 ± 0.8		
		Nov 20	51,868	0.18	19.72	79.59	54.6 ± 0.5		
		Nov 20	51,868	0.18	19.72	79.86	56.1 ± 0.5		
		Nov 23	51,871	0.19	32.31	78.99	29.3 ± 1.0		
		Nov 23	51,871	0.19	32.33	79.94	29.4 ± 0.9		
		Nov 23	51,871	0.19	32.34	80.71	32.0 ± 1.0		
		$\alpha$ Cet .....	Mira M7 IIIe	Nov 14	51,862	0.10	23.35	105.91	37.4 ± 0.5
Nov 15	51,863			0.10	22.49	95.51	41.9 ± 1.2		
Nov 18	51,866			0.11	22.38	89.11	41.0 ± 0.9		
Nov 18	51,866			0.11	22.38	89.53	41.7 ± 1.0		
Nov 20	51,868			0.12	17.28	63.17	55.3 ± 0.7		
Nov 20	51,868			0.12	17.01	64.86	58.1 ± 0.6		
Nov 23	51,871			0.13	25.79	64.23	30.6 ± 0.8		
Nov 23	51,871			0.13	25.67	64.75	31.4 ± 0.8		
R Cnc.....	Mira M7 IIIe			Nov 20	51,868	0.06	20.04	58.05	94.0 ± 2.1
				Nov 20	51,868	0.06	20.03	58.22	88.0 ± 2.4
RS Cnc.....	S M6 IIIa se			Nov 17	51,866	0.83	27.28	93.20	73.3 ± 3.9
		Nov 17	51,866	0.83	27.28	71.33	73.0 ± 2.5		
		Nov 19	51,867	0.85	20.30	71.33	93.0 ± 2.5		
		Nov 19	51,867	0.85	20.30	71.69	88.7 ± 2.3		
		Nov 19	51,867	0.85	20.29	72.01	90.2 ± 2.6		
		Nov 20	51,869	0.86	20.21	58.85	92.1 ± 1.0		
		Nov 20	51,869	0.86	20.23	59.52	90.8 ± 0.9		
		Nov 22	51,871	0.88	32.81	60.83	75.8 ± 2.0		
		Nov 22	51,871	0.88	32.80	61.17	71.1 ± 1.7		
		$\chi$ Cyg.....	Mira S	Nov 14	51,862	0.80	27.11	109.13	43.7 ± 0.5
Nov 14	51,862			0.80	27.00	111.90	42.8 ± 0.4		
Nov 20	51,868			0.82	20.25	94.40	53.6 ± 0.7		
Nov 20	51,868			0.82	20.25	95.05	52.5 ± 0.7		
Nov 20	51,868			0.82	20.27	99.17	53.6 ± 0.9		
Nov 20	51,868			0.82	20.27	99.46	52.7 ± 0.9		
Nov 23	51,871			0.83	32.39	85.49	45.1 ± 1.6		
Nov 23	51,871			0.83	32.38	85.98	43.2 ± 1.6		

and November, which is not the case for the lower ones. This could be explained by the fact that the smallest structures in the envelope would vary less with the phase than the largest ones. Of course, this hypothesis should be tested with data acquired at other spatial frequencies in order to complete the visibility curve and precise its shape, as well as at other phases to check this possible behavior on the smallest scales.

#### 5.1.2. $\alpha$ Cet, R Cas, and $\chi$ Cyg

The stars  $\alpha$  Cet and R Cas show a deviation from a UD that can be explained by an extended envelope. This effect is far stronger for  $\chi$  Cyg, whose visibility curve departs a lot from a UD model beyond about 30 cycles arcsec<sup>-1</sup>. Further studies are required in order to better understand the exact geometry of the circumstellar environment of this star.

#### 5.1.3. R Cnc

R Cnc was observed in both runs and shows important variations in its diameter from  $16.59 \pm 0.42$  to  $13.39 \pm 2.45$  mas. One may notice that the closer to its visible maximum

this star was observed, the smaller the computed diameter was.

#### 5.1.4. U Ori

Measurements for U Ori were only done at low and intermediate spatial frequencies, and it is possible that a diffusing envelope has no impact on the visibility curve at those scales.

#### 5.1.5. R Aqr, R Lep, R LMi, and U Her

Since measurements were only done at one single spatial frequency for R Aqr, R Lep, R LMi, and U Her, only single-parameter models can be computed from those data, so that no conclusion can be drawn on the pertinence of the UD model.

### 5.2. Semiregular Variables

#### 5.2.1. RS Cnc

This star was observed in both runs and shows important variations in its diameter from  $21.71 \pm 1.09$  to  $14.81^{+3.22}_{-2.93}$  mas. However, the results should be taken with

TABLE 5  
2000 NOVEMBER DATA POINTS (FROM R LEO TO  $\rho$  PER)

Star	Spectral Type	UT Date	Julian Date	Phase	Spatial Frequency (cycles arcsec <sup>-1</sup> )	Azimuth (deg)	Visibility (%)
R Leo.....	Mira M8 IIIe	Nov 14	51,863	0.61	25.56	87.94	22.0 ± 0.5
		Nov 15	51,864	0.61	25.69	82.66	22.1 ± 0.6
		Nov 15	51,864	0.61	25.56	88.48	21.0 ± 0.5
		Nov 15	51,864	0.61	25.56	88.75	21.7 ± 0.6
		Nov 18	51,867	0.62	25.59	86.33	24.6 ± 0.8
		Nov 18	51,867	0.62	25.58	86.73	24.1 ± 0.8
		Nov 19	51,868	0.63	20.24	55.40	41.8 ± 0.9
		Nov 19	51,868	0.63	20.22	55.69	39.9 ± 0.8
		Nov 19	51,868	0.63	19.68	61.57	40.7 ± 0.8
		Nov 19	51,868	0.63	19.66	61.83	40.2 ± 0.7
		Nov 20	51,869	0.63	20.02	58.04	39.3 ± 0.3
		Nov 20	51,869	0.63	20.01	58.23	38.0 ± 0.4
		Nov 22	51,871	0.64	30.98	60.36	8.3 ± 0.4
		R Lep.....	Mira C IIe	Nov 20	51,869	0.41	12.87
Nov 20	51,869			0.41	12.83	74.05	72.2 ± 1.9
R LMi.....	Mira M7e	Nov 20	51,869	0.08	20.22	62.59	77.1 ± 1.5
		Nov 20	51,869	0.08	20.23	62.79	79.7 ± 1.3
$\alpha$ Ori.....	SR M1	Nov 15	51,863	...	24.89	94.97	11.9 ± 0.3
		Nov 15	51,863	...	24.91	95.47	11.8 ± 0.2
		Nov 20	51,868	...	19.44	60.17	36.3 ± 0.3
		Nov 20	51,868	...	19.41	60.39	36.7 ± 0.3
		Nov 23	51,872	...	27.15	81.31	7.5 ± 0.2
		Nov 23	51,872	...	27.12	81.93	7.3 ± 0.2
U Ori.....	Mira M8 III	Nov 23	51,872	...	27.08	82.55	8.0 ± 0.3
		Nov 15	51,863	0.96	26.94	103.08	50.2 ± 2.2
		Nov 15	51,864	0.96	27.10	107.81	47.4 ± 1.6
		Nov 20	51,868	0.97	20.33	56.64	73.4 ± 1.3
$\rho$ Per.....	SR M4 II	Nov 20	51,868	...	20.33	56.79	72.0 ± 1.5
		Nov 20	51,868	...	20.28	73.14	88.2 ± 0.9
		Nov 20	51,868	...	20.29	73.40	89.1 ± 0.9

some care, since they are based on one point only in March, and in November they depart quite a lot from a UD diameter curve. Further measurements are thus necessary. However, one may still notice that the closer to its

visible maximum this star was observed the smaller the computed UD was.

### 5.2.2. Other Semiregular Variables

Only one data point is available for g Her and RT Vir, so no conclusion can be drawn, nor for  $\rho$  Per, for which visibilities were acquired at only one spatial frequency. RX Boo and SW Vir, from this point of view, are a bit better, yet the spatial resolution provided by IOTA is not sufficient to explore the high spatial frequency part of their visibility curves.

TABLE 6  
BEST-FITTING UD DIAMETERS

Star	Mean Julian Date	UD (mas)
R Aqr.....	51,868	34.32 ± 1.09 <sup>a</sup>
RX Boo.....	51,615	21.00 ± 0.27 <sup>b</sup>
R Cnc.....	51,614	16.59 ± 0.42
	51,868	13.39 ± 2.45 <sup>b</sup>
RS Cnc.....	51,517	21.71 ± 1.09 <sup>a</sup>
$\alpha$ Her.....	51,615	31.04 ± 0.26 <sup>b</sup>
g Her.....	51,616	20.84 ± 0.59 <sup>a</sup>
U Her.....	51,614	14.26 ± 0.47
R Lep.....	51,869	37.11 ± 2.21 <sup>b</sup>
R LMi.....	51,869	21.44 ± 0.70 <sup>b</sup>
$\alpha$ Ori.....	51,616	42.73 ± 0.10 <sup>b</sup>
	51,868	42.17 ± 0.32 <sup>b</sup>
$\rho$ Per.....	51,868	15.26 ± 0.45
U Ori.....	51,866	25.66 ± 0.69 <sup>b</sup>
RT Vir.....	51,614	16.24 ± 0.73 <sup>a</sup>
SW Vir.....	51,615	22.88 ± 0.33 <sup>b</sup>

NOTE.—The table contains the best-fitting UD diameters for the stars for which no departure from the model is noticeable in the data

<sup>a</sup> Only one data point is available.

<sup>b</sup> The error bars were increased in order to reduce the  $\chi^2$  of the fit to one.

TABLE 7  
SMALLEST UD DIAMETER, BEST-FITTING UD, AND GREATEST UD DIAMETER FITTING

Star	Mean Julian Date	$\phi_{\min}$ (mas)	$\phi_{L'}$ (mas)	$\phi_{\max}$ (mas)
R Cas.....	51,867	26.78	31.09	33.67
$\sigma$ Cet.....	51,867	33.94	35.21	37.96
RS Cnc.....	51,868	11.88	14.81	18.03
$\chi$ Cyg.....	51,867	23.12	30.40	33.70
R Leo.....	51,615	35.50	36.02	36.45
	51,867	35.78	39.08	40.57

NOTES.—The table contains the smallest UD diameter fitting at least one data point, the best-fitting UD, and the greatest UD fitting at least one data point for the stars for which a strong departure from a UD model is noticeable in the data.

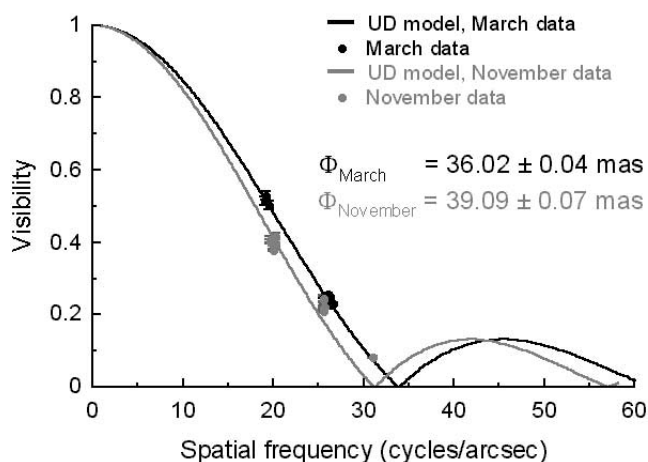


FIG. 7.—Visibility curves for R Leo in March and November

### 5.3. Supergiants

#### 5.3.1. $\alpha$ Ori

The star  $\alpha$  Ori had already been observed with TISIS, as reported by Mennesson et al. (2000), who gives a diameter of  $40.2 \pm 0.2$  mas. The quality of the present data is better, in particular because of the better sampling of the thermal background. Both diameters measured in March and November are roughly equivalent and do not show any significant variation in the size of the star, nor do they show an important discrepancy with the previous TISIS estimates of the diameter of  $\alpha$  Ori.

#### 5.3.2. $\alpha$ Her

TISIS observations of  $\alpha$  Her have already been reported by Mennesson et al. (1999), with an estimate of the diameter of  $32.8 \pm 0.7$  mas for data acquired in 1998 March to be compared with the  $31.04 \pm 0.08$  mas of the present work. This small variation may not be significant, since the observations of Mennesson et al. (1999) were the very first ones to be carried out with the instrument, of which we have now a better understanding.

## 6. CONCLUSION

After the first observations, which were reported in Mennesson et al. (1999), and the first attempts to implement a chopping system on IOTA in 2000 March, the instrument has proven in 2000 November its stability. It could then be regarded as fully operational and able to provide reproducible data of good quality. The present article will thus serve as a database for later publications. Further observations are needed to help determine the characteristics of a few stars, especially on shorter baselines for stars like  $\chi$  Cyg, whose curve shows a very interesting feature that should be investigated, or on longer baselines for stars like RS Cnc. Moreover, in most cases, as soon as data are available at higher spatial frequencies, departures from the UD model are more likely to occur. Some stars show a very important difference in their  $K'$ - and  $L'$ -band UD diameters, an effect that we are currently trying to understand (Mennesson et al. 2002). More detailed modeling of these objects requires multiplying the observations at different phases and at different spatial frequencies.

## REFERENCES

- Burns, D., et al. 1998, MNRAS, 297, 462  
 Colavita, M. M., et al. 1998, Proc. SPIE, 3350, 776  
 Coudé du Foresto, V., Perrin, G., Ruilier, C., Mennesson, B., Traub, W. A., & Lacasse, M. G. 1998, Proc. SPIE, 3350, 856  
 Coudé du Foresto, V., Ridgway, S., & Mariotti, J.-M. 1997, A&AS, 121, 379  
 Danchi, W. C., Bester, M., Degiacomi, C. G., Greenhill, L. J., & Townes, C. H. 1994, AJ, 107, 1469  
 di Benedetto, G. P., & Rabbia, Y. 1987, A&A, 188, 114  
 Gilliland, R. L., & Dupree, A. K. 1996, ApJ, 463, L29  
 Hale, D. D. S., et al. 2000, ApJ, 537, 998  
 Léger, A., Mariotti, J. M., Mennesson, B., Ollivier, M., Puget, J. L., Rouan, D., & Schneider, J. 1996, Ap&SS, 241, 135  
 Leinert, C., & Graser, U. 1998, Proc. SPIE, 3350, 389  
 Manduca, A. 1979, A&AS, 36, 411  
 Mennesson, B., et al. 1999, A&A, 346, 181  
 ———. 2002, ApJ, in press  
 Mennesson, B., et al. 2000, Proc. SPIE, 4006, 481  
 Perrin, G., Coudé du Foresto, V., Ridgway, S. T., Mariotti, J.-M., Traub, W. A., Carleton, N. P., & Lacasse, M. G. 1998, A&A, 331, 619  
 Perrin, G., Coudé du Foresto, V., Ridgway, S. T., Mennesson, B., Ruilier, C., Mariotti, J.-M., Traub, W. A., & Lacasse, M. G. 1999, A&A, 345, 221  
 Thompson, R. R., Creech-Eakman, M. J., & van Belle, G. T. 2002, ApJ, submitted  
 Traub, W. A. 1998, Proc. SPIE, 3350, 848  
 Tuthill, P. G., Haniff, C. A., & Baldwin, J. E. 1999a, MNRAS, 306, 353  
 Tuthill, P. G., Monnier, J. D., & Danchi, W. C. 1999b, in ASP Conf. Ser. 194, Working on Fringe: Optical and IR Interferometry from Ground and Space, ed. S. C. Unwin & R. Stachnik (San Francisco: ASP), 188  
 ———. 2000, Proc. SPIE, 4006, 491  
 Tsuji, T., Ohnaka, K., Aoki, W., & Yamamura, I. 1997, A&A, 320, L1  
 Yamamura, I., de Jong, T., & Cami, J. 1999, A&A, 348, L55  
 Young, J. S., et al. 2000, MNRAS, 315, 635